OsteoArthritis and Cartilage (2006) **14,** 215–223

doi:10.1016/j.joca.2005.09.008

Osteoarthritis and Cartilage

International Cartilage Repair Society

OARSI OSTEOARTHRITIS RESEARCH SOCIETY INTERNATIONAL

Subchondral bone micro-architectural alterations in osteoarthritis: a synchrotron micro-computed tomography study

Dr. C. Chappard Ph.D., M.D.*, F. Peyrin Ph.D., A. Bonnassie Ph.D., G. Lemineur Ph.D., B. Brunet-Imbault Ph.D., E. Lespessailles M.D. and C.-L. Benhamou M.D.
Inserm, U 658, Centre Hospitalier Orleans, IPROS I rue porte madeleine, 45032 Orleans, France

Summary

Objectives: We evaluated the three-dimensional (3D) micro-architecture of subchondral trabecular (Tb) bone in osteoarthritis (OA). Due to high signal-to-noise ratio and high resolution, micro-computed tomography (micro-CT) by synchrotron radiation is considered as the gold standard for bone micro-architecture imaging.

Design: Subchondral bone were extracted from femoral heads in OA cases in areas without cartilage (OAc−; $n = 6$) and in adjacent areas with cartilage (OAc+; $n = 6$) and compared to eight subchondral bone cores from osteoporosis cases (OP). The voxel size of images was 10.13 μm. We measured the bone volume fraction (BV/TV) and morphological parameters: Tb thickness (TbTh), Tb spacing (TbSp), Tb number (TbN), and bone surface/bone volume (BS/BV). The degree of anisotropy (DA), the connectivity by the Euler number and the degree of mineralization (DM) were equally assessed.

Results: BV/TV and morphological parameters showed significant differences between OAc− and OP samples ($P < 0.01$ except TbTh: $P < 0.05$) and between OAc− and OAc+ ($0.05 < P < 0.01$) but no difference between OAc+ and OP except TbN ($P < 0.01$). The connectivity was higher in OAc− comparatively to OAc+ and OP. The DA were significantly different between OA and OP cases ($P < 0.01$) but not between OAc− and OAc+ specimens. The DMs (mean ± SD) were 0.817 ± 0.142 g/cm^3, 0.873 ± 0.161 g/cm^3, 0.906 ± 0.156 g/cm^3 for OAc−, OAc+, OP ($P < 0.01$), respectively.

Conclusion: Subchondral bone changes were mainly observed in advanced OA, when cartilage has been deleted and preserved in adjacent area. These data suggest that subchondral bone changes would be rather secondary to the cartilage deterioration than a primitive mechanism of OA. Nevertheless, longitudinal data could bring more accurate conclusions.

Key words: Subchondral bone, Trabecular bone micro-architecture, Micro-computed tomography, Synchrotron radiation.

Introduction

Osteoarthritis (OA) and osteoporosis (OP) are common afflictions of aged human beings. OP is more rarely found in patients with OA than in controls and *vice et versa*[1]. Recently, the relationship between OP and OA was not described as a simple inverse association[2]. OA is characterized by the progressive destruction of articular cartilage and changes in subchondral bone. Bone changes surrounding the OA joint are frequently seen on radiographs of OA patients. The sclerosis of the subchondral bone is regarded as one of the primary radiologic features of OA[3]. The relationship between bone and cartilage in OA has been widely discussed[4]. Although the destruction of articular cartilage is indeed the main feature of OA, some researchers suspected the subchondral bone of exacerbating the degeneration. Repetitive impact loading has been shown to induce subchondral bone changes resulting in a less compliant trabecular (Tb) bone which thereby transfers excessive mechanical stress to the overlying articular cartilage[5]. The question of whether the subchondral changes occur before cartilage deterioration or are subsequent to these changes still remains unanswered[6]. Some authors observed a thickening of the subchondral bone preceeding alteration of the cartilage[7,8]. Others observed that thickening of the subchondral bone was not required to initiate cartilage fibrillation and there was only osteophyte formation[9]. Some authors have underlined the usefulness of antiresorptive therapies to reduce the progression of OA[10].

Subchondral bone changes have been already evaluated by histomorphometry in OA animal models[11,12] and from humans with OA[13–16]. The latter author concludes that more precise analysis with regional distribution of bone parameters is very important for a better understanding of subchondral bone structural changes due to the disease[16]. Indeed, in conventional histology, a long preparation is necessary and the histological cutting process may cause mechanical deformations and cracks[17]. There is no three-dimensional (3D) representation, the stereological interpretation of two-dimensional (2D) slices remains very controversial[18]. The subchondral bone micro-architecture changes have been evaluated with 3D micro-computed tomography (micro-CT) in animal models[7,9,19] with voxel sizes ranging from 30 to 60 μm. Micro-CT images were also performed in human tibia with and without OA with a 22 μm voxel size[20]. However, to assess the bone morphometric parameters, the most appropriate voxel size is around 10 μm[21]. All previous studies have been performed

*Address correspondence and reprint requests to: Dr Christine Chappard, Ph.D., M.D., Inserm, U 658, Centre Hospitalier Orleans, IPROS I rue porte madeleine, 45032 Orleans, France. Tel: 33-238744053; Fax: 33-238744024; E-mail: christine.chappard@chr-orleans.fr
Received 3 January 2005; revision accepted 21 September 2005.

with conventional desktop micro-CT. The synchrotron radiation (SR) micro-CT presents substantial advantages. The X-ray beam chosen may be monochromatic and nondivergent. The high signal-to-noise ratio in the SR micro-CT image is of interest for the segmentation of bone from the background, and this technique also permits the assessment of mineralization variations. SR micro-CT is considered as the most accurate technique for quantifying both the mineralization at the trabeculae level and the micro-architecture on the same sample[22]. SR micro-CT systems have already been applied to bone studies to observe OP alterations and medication effects[16,23–27]. At this time, SR micro-CT is considered as a gold standard to evaluate the 3D micro-architecture of Tb bone[26].

The aim of this study was to evaluate alterations of subchondral Tb bone on human femoral heads in relation to OA by comparison with OP using SR micro-CT. We compared OA subchondral Tb bone in areas with full thickness loss (OA without cartilage, OAc−) without cartilage considered as the last stage of the disease with adjacent subchondral Tb bone in areas surrounded by cartilage considered as an earlier stage of the disease.

Materials and methods

SPECIMENS

The bone subchondral specimens were sampled from femoral heads removed during arthroplasty for six OA and eight OP cases in male patients (Orthopedic Surgery Department of Centre Hospitalier d'Orleans). Patients with congenital or acquired dysplasia, or avascular necrosis were excluded from the OA group. Patients with osteomalacia, multiple myeloma, rheumatoid arthritis or secondary OP due to corticosteroids were excluded from the OP group. The mean age was 66.5 ± 15.9 years for OA patients and 79.1 ± 13.0 years for OP patients ($P = 0.08$). All bone cores were always sampled in the long axis of the femoral neck perpendicular to the surface in the superior area near the fovea. The ''osteoporotic'' bone cores were always sampled on the meridian line. In each ''osteoarthritic'' femoral head, two subchondral bone cores were obtained: one without cartilage (OAc−) and the other with cartilage (OAc+) either on the anterior area, or on the meridian line or on the posterior area. The details are described in Fig. 1. The cylindrical cores of subchondral bone with size of 10 mm height and 8 mm in diameter were prepared under continuous water irrigation using a precision diamond circular saw. All the samples comprised the subchondral Tb bone immediately under cartilage and subchondral cortical bone. They were chemically defatted (several cycles of submerging in bleach and dichloromethane) in order to remove the bone marrow[28]. Typical subchondral bone cores are represented in Fig. 2.

IMAGE ACQUISITION

The 14 cleaned bone cores were imaged using SR at the European Synchrotron Radiation Facility (ESRF, Grenoble, France) on beamline ID19. The set-up provides a very intense, homogeneous, parallel and monochromatic beam. The detailed description of the device has been previously reported[29]. The transmitted X-ray beam was recorded with a scintillator coupled to a 2D 1024 × 1024 Coupled Charge Device (CCD) camera with a dynamic range of 14 bits developed by the ESRF Detector Group. For these experiments, the X-ray energy was set at 20 keV for the OP

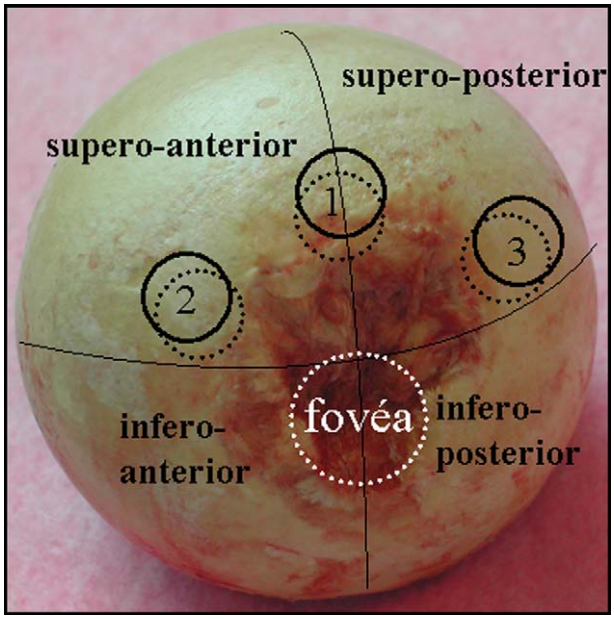

Fig. 1. Location of bone cores. The osteoporotic bone cores were always sampled in position 1. OA bone cores were sampled in area with and without cartilage according to locations 1, 2, and 3.

samples and 23 keV for the OA samples. To perform a flat field correction, dark, current and reference images without the sample were taken regularly during the acquisition. With an angular step of 0.2° over an angular range of 180°, 900 radiographic projections were acquired. The exposure time for one image was about 0.3 s, thus the total scan of each sample was about 15 min. The optical system was set to get a pixel size of 10.13 μm.

The calibration method to estimate the 3D distribution of mineral content within the bone sample was previously described[22].

IMAGE PROCESSING

The 3D bone structure was reconstructed from a set of 2D radiographic projections under different angles of view with an exact tomographic reconstruction algorithm based on 3D filtered back-projection (Ram-Lak filter). Typical 3D images obtained with SRs are illustrated in Fig. 3.

A cylinder region of interest (ROI) of 580 pixels diameter × 600 was selected and centred inside bone (corresponding to 5.875 mm and 6.078 mm, respectively). A preliminary treatment was used to remove isolated bone and marrow particles. These isolated Tb bone parts have been demonstrated to have no significant influence from a mechanical point of view[30]. The 3D reconstructed volumes were segmented by a global threshold above which all voxels are considered as bone and below which all voxels are considered as background. An identical global threshold for each group (OA and OP) was performed to binarize images. An example of binarized image is reported in Fig. 4.

MEASURED AND CALCULATED PARAMETERS

Morphological and topological parameters were then computed from the 3D binarized volumes with software tools developed at CREATIS. Morphometric parameters

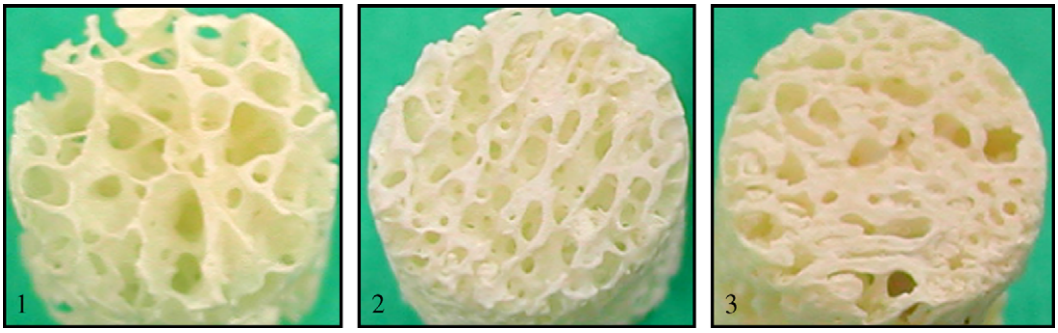

Fig. 2. Typical bone cores obtained after deffating. (1) OP sample; (2) OA sample with cartilage; and (3) OA sample without cartilage.

were computed by using the mean intercept length (MIL) technique[31]. The bone volume/tissue volume (BV/TV) corresponding to the bone proportion was measured. A random set of test lines was used, and the number of intersections of lines with bone boundaries was evaluated. The Tb number (TbN, mm^{-1}), is then given by:

$$\mathrm{TbN}\left(mm^{-1}\right) = \text{Intercept number}/\text{parallel test line length} \quad (1)$$

The Tb spacing (TbSp, μm), the Tb thickness (TbTh, μm) and the bone surface/bone volume (BS/BV, mm^{-1}) are then derived from BV/TV and TbN measured according to a parallel plate model[32]. To avoid any model hypothesis, we also used a direct method proposed by Hildebrand *et al.*[33]. This method enables to estimate the distribution of TbTh on the whole volume, and then the mean TbTh* (μm). We proposed an implementation of the method based on 3D discrete Chamfer distance and medial axis transformation[34].

The MIL method also enables to define the principal orientation of the structure by fitting the degree of anisotropy (DA, no unit), defining the orientation of the structure[35]. For each direction, the number of intersections normalized by length of the test line was represented by a point in 3D space. All these points may then be fitted by an ellipsoid, the half axes of which taken in descending order are called MIL1, MIL2, MIL3. The 3D anisotropy degree is then estimated by

$$\mathrm{DA} = \mathrm{MIL1}/\mathrm{MIL3} \quad (2)$$

DA equals one for isotropic structure, the higher the DA, the more anisotropic the structure.

The connectivity was quantified by the Euler number (χ). There is a simple method to calculate the Euler number by computing the meeting points between two voxels: n_0 = number of vertexes, n_1 = number of edges, n_2 = number of faces, and n_3 = number of voxels. The Euler number is obtained by the following formula:

$$\chi = n_0 - n_1 + n_2 - n_3 \quad (3)$$

If the object is made of a single connected component and contains no voids, the connectivity may be quantified by the Betti number β_1 and is related to the Euler number by the following formula:

$$\chi = 1 - \beta_1 \quad (4)$$

A highly connected structure, such as healthy cancellous bone has a high negative Euler number and an OP bone has an absolute smaller value. This method was previously described in detail by Odgaard and Gundersen[18] for bone applications.

The grey levels corresponding to bone absorption were converted into concentrations of mineral content in g/cm^3 according to the calibration method. The procedure is previously described[22].

DATA ANALYSIS

All statistical computations were done with NCSS (Kaysville, USA). An analysis of variance (ANOVA) test was used to compare the three groups.

For morphological and topological parameters, a Wilcoxon signed rank test was used to compare OA specimens with cartilage and without cartilage from the same femoral heads. A Mann–Whitney rank test was used to compare

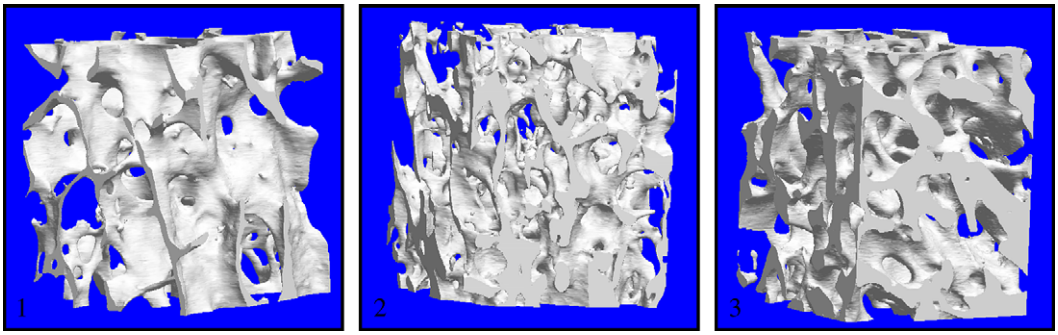

Fig. 3. Typical 3D images obtained with synchrotron imaging of bone samples. The voxel size is isotropic, 10.13 μm. (1) OP sample; (2) OA sample with cartilage; and (3) OA sample without cartilage.

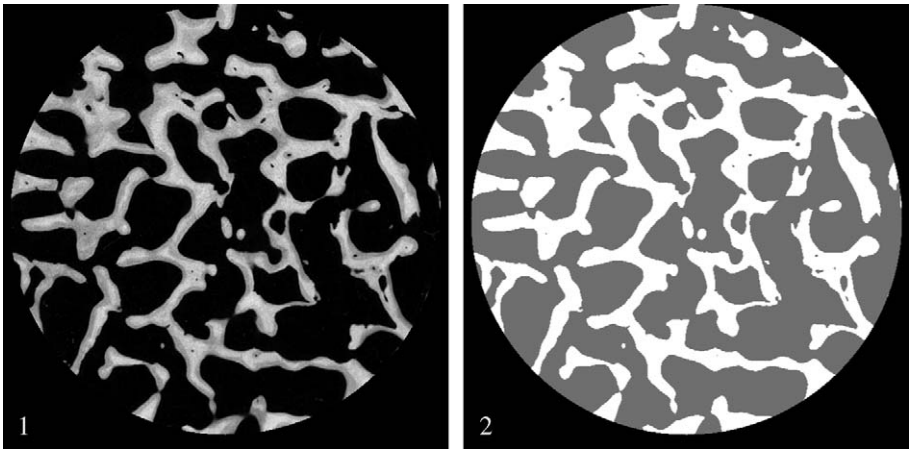

Fig. 4. Example of a synchrotron reconstruction obtained before and after binarization. (1) Grey level image; (2) white colour = Tb bone and grey colour = inter-TbSp.

OP and OA specimens. An analysis of covariance with age as covariate was used to compare the parameters from OA and OP groups.

For each bone morphologic parameter, we calculated the average percentage deviation from OAc+ subchondral Tb bone comparatively to the OAc− subchondral Tb bone.

$$\langle \Delta \text{bone parameter} \rangle = \frac{100}{n} \sum_{i=1}^{i=n} \frac{\text{bone parameter}(\text{OAc}+)_i - \text{bone parameter}(\text{OAc}-)_i}{\text{bone parameter}(\text{OAc}-)_i} \quad (5)$$

where n is the number of specimens.

The distribution of grey levels within the different ROIs was obtained from the histogram of the bone images normalized by the total volume. The histograms were averaged for each group.

Results

Morphological parameters for OP, OAc+ and OAc− subchondral bone samples are described in Table I and illustrated in Fig. 5. Topological parameters are represented in Table I and illustrated in Fig. 6. All morphological and topological parameters were different according to ANOVA tests. All morphological and topological parameters showed statistically significant difference between OAc− and OP samples (with $P < 0.01$ except TbTh: $P < 0.05$). The differences in morphological parameters such as BV/TV, BS/BV, TbTh, TbTh*, TbSp were statistically significant between OA samples with and without cartilage ($0.05 < P < 0.01$). These parameters were not significantly different between OAc+ and OP except TbN ($P < 0.01$).

Concerning topological parameters, higher connectivity was found in OAc− subchondral bone samples comparatively to OAc+ and OP subchondral bone samples. Moreover, the connectivity was also higher in OAc+ subchondral bone samples comparatively to OP samples. For DA parameter, there were significant differences between OA samples and OP samples ($P < 0.01$). In both

Table I
Bone morphological parameters: mean, standard deviation (SD) and range of variation concerning subchondral bone for OP, OA with cartilage (OAc+) and without cartilage (OAc−). ANOVA test was used to compare groups

	OAc− ($n = 6$), mean ± SD [range]	OAc+ ($n = 6$), mean ± SD [range]	OP ($n = 8$), mean ± SD [range]	ANOVA P
BV/TV (%)	35.9 ± 7.0 [31.3, 49.8]	21.7 ± 5.3 [15.4, 30.5]	18.3 ± 4.6 [11.9, 24.7]	6×10^{-5}
BS/BV (mm^{-1})	13.12 ± 2.48 [9.57, 15.50]	18.3 ± 2.5 [14.8, 21.3]	17.44 ± 2.76 [12.75, 21.36]	6×10^{-3}
TbTh (μm)	157.6 ± 33.1 [129.0, 208.9]	110.9 ± 16.1 [93.8, 135.2]	117.4 ± 19.9 [93.6, 156.9]	6×10^{-3}
TbTh* (μm)	235.5 ± 42.2 [193.1, 298.6]	172.2 ± 19.3 [148.0, 195.3]	170.8 ± 25.9 [135.4, 219.1]	10^{-3}
TbSp (mm)	0.28 ± 0.06 [0.21, 0.36]	0.41 ± 0.07 [0.29, 0.51]	0.54 ± 0.11 [0.40, 0.71]	10^{-4}
TbN (mm^{-1})	2.30 ± 0.33 [1.81, 2.72]	1.94 ± 0.29 [1.64, 2.43]	1.55 ± 0.25 [1.23, 1.91]	5×10^{-4}
Euler (mm^{-3})	−20.5 ± 11.3 [−34.2, −5.6]	−12.7 ± 11.5 [−35.9, −5.5]	−5.6 ± 2.5 [−8.5, −2.7]	2×10^{-5}
DA	1.38 ± 0.09 [1.25, 1.46]	1.40 ± 0.14 [1.12,1.53]	1.64 ± 0.10 [1.48, 1.76]	6×10^{-4}

TbTh* was measured by the Hildebrand method.

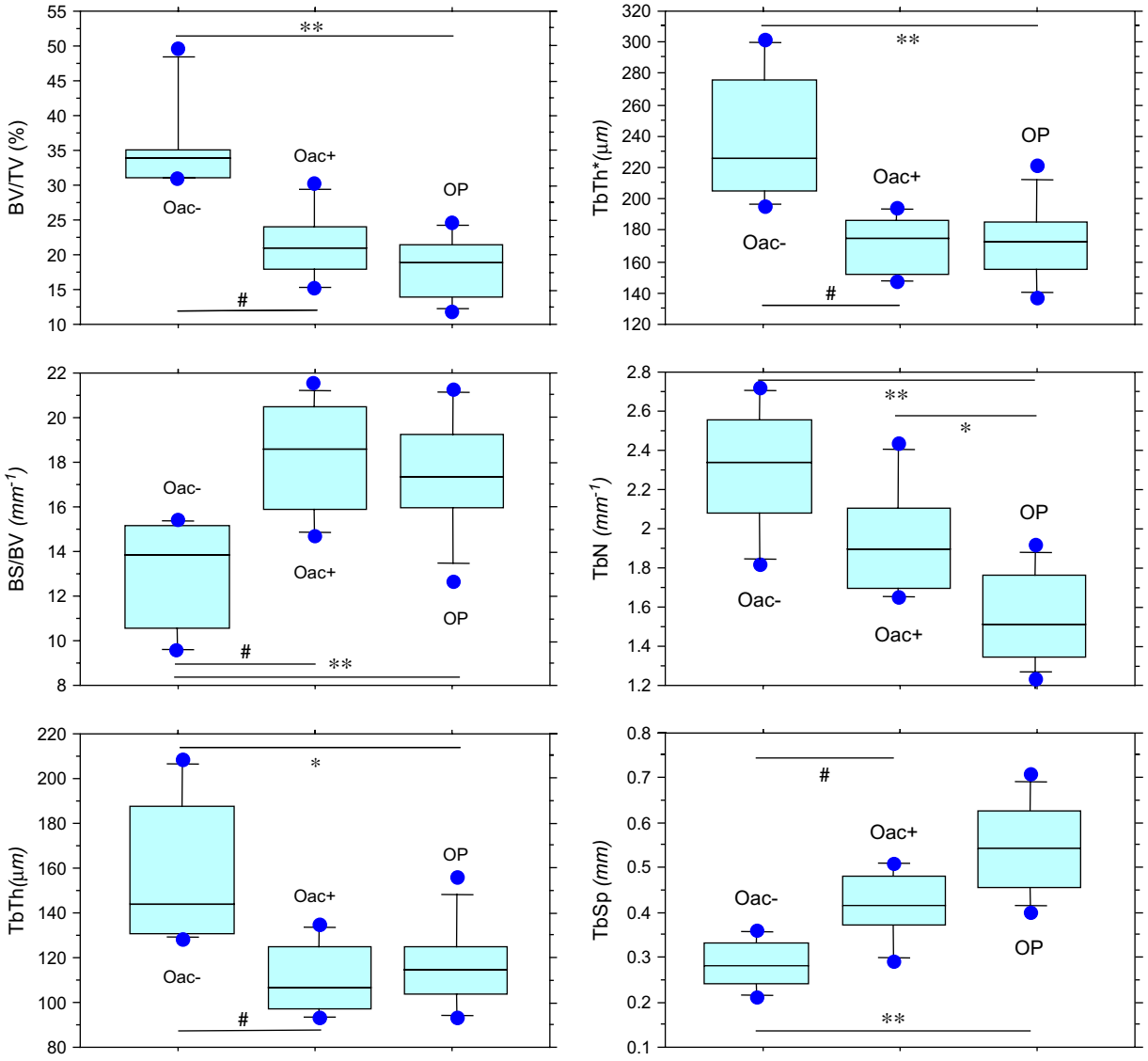

Fig. 5. Results of morphological parameters for OA subchondral bone samples with cartilage (OAc+) and without cartilage (OAc−) from the same femoral heads and OP subchondral bone samples (OP). *$P < 0.05$ and **$P < 0.01$ with a Mann–Whitney test, #$P < 0.05$ with a Wilcoxon test.

cases, there was no difference between OAc− and OAc+ specimens. When adjusted for age, there was no difference between OAc+ and OP (data not shown) except for DA, the mean ± standard error was 1.40 ± 0.05 and 1.64 ± 0.04 for OAc+ and OP ($P < 0.01$), respectively. All parameters remained significantly different between OAc− group and OP group ($0.05 < P < 0.0005$).

The results of the intra-individual variations represented by the individual mean variations in percentage between OAc− and OAc+ and the estimation of the inter-individual variations by the mean differences between OAc+ and OP are shown in Table II. The intra-individual differences were high, ranging from +14.9% to +39.5% for TbN and BV/TV, respectively and were −43.6% and −46.9% for BS/BV and TbSp, respectively. These intra-individual differences were higher than the inter-individual differences for all parameters except for TbN.

The mean distribution of the degree of mineralization is shown in Fig. 7. The degree of mineralization (mean ± SD) of bone samples was 0.817 ± 0.142 g/cm^3, 0.873 ± 0.161 g/cm^3, and 0.906 ± 0.156 g/cm^3 for OAc−, OAc+, and OP, respectively. The P value of OAc+ vs OAc− obtained by the Wilcoxon test was 0.005. The P values of OAc+ vs OP and OAc− vs OP obtained with the Mann–Whitney test were 0.002 and 0.01, respectively. Bone specimens from OA femoral heads without cartilage are hypomineralized and more heterogeneous comparatively to those covered by cartilage and to OP cases.

Discussion

This is the first study investigating micro-architectural characterization of human subchondral Tb bone in OA by SR micro-CT. We observed that subchondral bone impairments are mainly observed in advanced OA, when cartilage has been deleted. These data suggest that these subchondral bone impairments would be a mechanism of OA rather

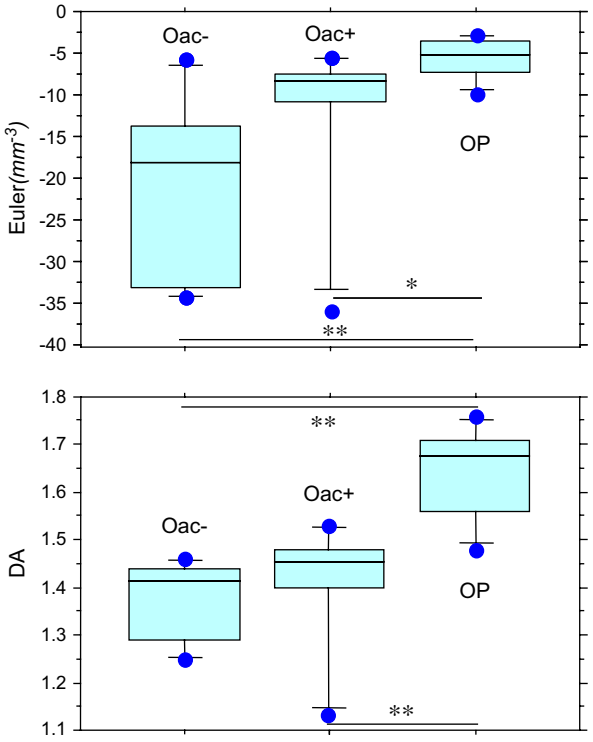

Fig. 6. Results of topological parameters for OA subchondral bone samples with cartilage (OAc+) and without cartilage (OAc−) from the same femoral heads and OP subchondral bone samples (OP). *$P < 0.05$ and **$P < 0.01$ with a Mann−Whitney test.

secondary to the cartilage deterioration than a primitive mechanism of OA. The intra-individual variations inside the femoral head were superior to the estimation of inter-individual variations between OA and OP samples suggesting that there were profound micro-architectural alterations in subchondral bone in response to cartilage degradation. In our study there was a difference in age between groups. The ages of OA and hip fracture groups were those found usually in literature[36]. However, the adjustment to age did not change the interpretation. These results suggest that the influence of environment loading in development and maintenance of micro-architectural alterations are more important than ageing at the femoral heads.

In OA, the mean BV/TV was increased in subchondral Tb bone area without cartilage comparatively to subchondral

Table II

Intra-individual variations expressed by the mean individual deviations in percentage of bone morphological parameters between Tb subchondral bone from OA cases with cartilage (OAc+) and without cartilage (OAc−) and an estimation of inter-individual variations expressed by the difference of the mean between (OAc+) and (OP)

	Mean Δ_i (%), OAc−/OAc+	Δ Mean (%), OAc+/OP
BV/TV (%)	+39.5	−15.8
BS/BV (mm^{-1})	−43.6	−4.8
TbTh (μm)	+27.5	+5.8
TbTh* (μm)	+26.5	+0.7
TbSp (mm)	−46.9	−31.5
TbN (mm^{-1})	+14.9	−20.4

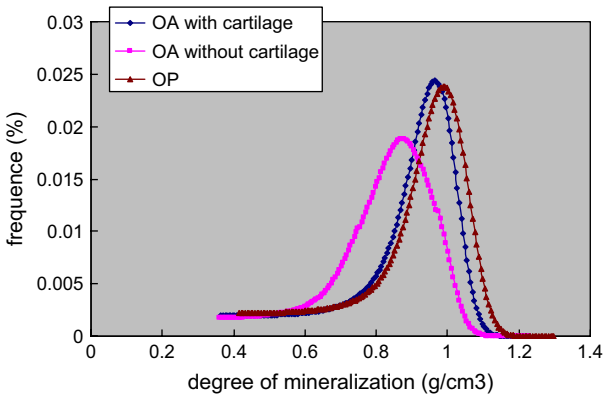

Fig. 7. Distributions of the degree of mineralization (g/cm^3) in osteoarthritic femoral heads with and without cartilage and in osteoporotic femoral heads.

adjacent Tb bone area covered by cartilage (35.1 ± 7% vs 21.7 ± 5.3%). The mean BV/TV of OP bone was close to subchondral bone with cartilage in OA (18.3 ± 4.6%. vs 21.7 ± 5.3%). There is agreement with most histomorphometric studies which have reported an increase in Tb bone volume in human bone with OA[13,15,16,37] or in animal models[11]. Fazzalari and Parkinson[13] measured BV/TV in two subchondral regions superior and infero-medial to the fovea from OA hip. They found BV/TV at 36.9% in the superior region and 15.8% in the infero-medial region. These results are close to ours where all bone cores were sampled in the superior regions of fovea. Li and Aspden[37] have reported a BV/TV increase of 60% in the OA group and a reduction of 18% in the OP group and considered that OP and normal bone are very similar in femoral heads.

With conventional micro-CT, Ding *et al.* found a significant increase of bone fraction in % in early OA comparatively to controls. Conventional micro-CT was also used to evaluate changes in subchondral bone at the femur in guinea pigs[7] and at the tibial plateau in dogs[9,38]. A discrepancy between these experiments has been observed. The BV/TV was increased in subchondral bone of experimental animals with OA comparatively to controls[7]. On the contrary, there is a trend to decrease in BV/TV at 18 and 54 months[9] and at 3 and 12 weeks after anterior cruciate ligament transection in dogs[38]. It is possible that in post-traumatic OA Tb micro-architecture changes are different than in primitive OA. Moreover, in human bone, only later stages of the disease are observable.

In our study, in OA without cartilage cases (OAc−), morphological parameters such as TbTh, TbTh* and TbN were higher and TbSp and BS/BV were smaller explaining the increase of BV/TV. These results suggest an uncoupled balance between bone resorption and bone formation with a predominant bone formation. In histomophometric studies, discordant results were found. For the highest stage of cartilage degeneration, Bobinac *et al.*[16] found in tibial plateaus a significant TbTh increase and a decrease in TbSp with no difference in TbN. Kamibayashi *et al.*[15] in subchondral bone of tibial plateaus found lesser, widely spaced and thicker trabeculae in OA comparatively to controls. In severe OA of femoral head removed during hip replacement surgery, Fazzalari and Parkinson[13] found that Tb volume increased mainly through an increase in TbN and reduced TbSp rather than a thickening of trabeculae. TbTh and BS/BV that we found are concordant with those in a conventional micro-CT

study performed in early OA whereas the TbN increase and TbSp decrease are more pronounced in our study performed at the later stage of OA. This observation might suggest that the increase of TbTh is an earlier phenomenon in reaction to cartilage degradation, the increase of TbN appearing secondarily. In animal models, the increasing subchondral bone fraction of experimental OA comparatively to controls was due to a significant decrease in TbSp and to a tendency to increase in TbTh and density[7]. On the contrary with the same technique, TbTh was decreased, BS/BV and TbSp went up and no detectable change was found in TbN[38].

In our study, the high Tb bone volume in OAc− might be due to an increase in TbTh in comparison with the area of the same femoral heads with cartilage (OAc+), the number of trabeculae increasing to a lesser extent. The differences in the number of trabeculae between OA and OP groups were probably due to a Tb deletion in the OP group and not only a real increase in OA. Indeed, the distribution of TbN values in OAc+ was intermediate between OAc− and OP groups and there was no difference between OAc− and OAc+ for this parameter. On the contrary, whatever the method of measurement (direct or indirect), TbTh and TbTh* in OAc+ group were close to TbTh and TbTh* in OP group.

We have found that a connectivity expressed by the Euler number increased in subchondral bone without cartilage. Various results about connectivity have been noticed. The 3D connectivity of Tb bone structure was increased early in both femur and tibia after unilateral anterior cruciate ligament transection[19]. Connectivity density was not modified in early OA of human tibias[19]. On the contrary, Kamibayashi *et al.* with histomorphometric methods on 2D slices reported that trabeculae are thicker and more widely spaced in human OA knees. They interpreted this data as an early loss of connectivity followed by a compensatory thickening of the remaining structure[15]. However, the stereological interpretation of 2D slices is considered to be very controversial[18]. From a stereological point of view, only 3D representation is reliable to measure the connectivity. In our case, the 3D connectivity density was measured in late OA but with a large variability between specimens explaining probably the lack of difference between OAc− and OAc+. We noticed that connectivity varied in parallel with the TbN parameter.

Local anisotropy of the cancellous bone structure was closely related to mechanical anisotropy[35]. The higher anisotropy found in OP bone cores suggested bone deletions in preferential directions as it was already suggested[39]. Few studies have described an increase in anisotropy in weight-bearing osteoporotic bones; this has been demonstrated at vertebrae[40], at femoral neck[41] and at calcaneus[42]. In our study, we found a tendency of a lower anisotropy in the absence of cartilage. Radin and Rose[43] have already suggested concerning OA subchondral bone a relationship between shear stresses and material anisotropy. We can imagine that the shear stresses propagated in parallel to the interface between cartilage and bone may initiate bone formation preferentially in a direction parallel to the bone surface and change the local anisotropy. In a prospective study, a decrease of anisotropy accompanied by bone structure changes in animals after anterior cruciate ligament transection was described[19].

The main strength of our study is that it was performed in an optimized way: defatted human bone specimens were imaged with voxel sizes approximately 10 times smaller than TbTh. A resolution around 10 μm was described necessary to identify bone micro-architecture with accuracy[21]. The SR micro-CT is considered as a gold standard for micro-computed imaging with high signal-to-noise ratio. With this technique the segmentation of bone from the background is simplified, a unique threshold being applied for the whole data set[21]. Indeed, with conventional micro-CT (polychromatic X-rays and cone beam geometry) the segmentation of bone tissue from marrow has been recognized by many authors to be a critical step to interpret morphological bone parameters[43–46].

Another strength of the SR micro-CT method is the possibility to evaluate the mineralization of trabeculae. We found OAc− bone specimens hypomineralized and more heterogeneous comparatively to OAc+ and OP cases. The heterogeneity of mineralization in trabeculae is probably a consequence of high level of bone remodeling[49]. Our results are in accordance with those obtained with different methods of measurements such as density fractionation on powdered bone[50], analysis of calcium content[46] and quantitative backscattered electron imaging[48]. In OA both weight-bearing and non-weight-bearing subchondral bones showed a lower degree of mineralization than age-matched controls and young controls.[47]. Defect in calcium content of collagen has been already reported in human bone with OA comparatively to controls[49].

In conclusion, we used the SR micro-CT considered as the most reliable technique at this time to assess bone micro-architecture. We have shown differences in bone micro-architecture in subchondral Tb bone area with full thickness loss of cartilage comparatively to a close area surrounded by cartilage. These results suggest that the increase in BV/TV is mainly due to TbTh and to a lesser extent to TbN and would be a secondary mechanism aiming to preserve mechanical properties of subchondral bone. However, in the absence of a longitudinal design, our results still do not definitely determine whether the alterations observed in OA bone are really secondary to degenerative changes in the cartilage.

References

1. Verstraeten A, Van Ermen H, Haghebaert G, Nijs J, Geusens P, Dequeker J. Osteoarthrosis retards the development of osteoporosis. Observation of the coexistence of osteoarthrosis and osteoporosis. Clin Orthop 1991;264:169–77.
2. Lane NE, Nevitt MC. Osteoarthritis, bone mass, and fractures: how are they related? Arthritis Rheum 2002;46:1–4. Review.
3. Resnick D. Diagnosis of Bone and Joints Disorders. 4th ed. Philadelphia, London: Saunders; 2002.
4. Burr DB. Anatomy and physiology of the mineralized tissues: role in the pathogenesis of osteoarthrosis. Osteoarthritis Cartilage 2004;12(Suppl A):S20–30.
5. Brown TD, Radin EL, Martin RB, Burr DB. Finite element studies of some juxtarticular stress changes due to localized subchondral stiffening. J Biomech 1984;17:11–24.
6. Lajeunesse D. The role of bone in the treatment of osteoarthritis. Osteoarthritis Cartilage 2004;12:S34–8.
7. Layton MW, Goldstein SA, Goulet RW, Feldkamp LA, Kubinski DJ, Bole GG. Examination of subchondral bone architecture in experimental osteoarthritis by microscopic computed axial tomography. Arthritis Rheum 1988;31:1400–5.
8. Carlson CS, Loeser RF, Jayo MJ, Weaver DS, Adams MR, Jerome CP. Osteoarthritis in cynomolgus

macaques: a primate model of naturally occurring disease. J Orthop Res 1994;12:331−9.
9. Dedrick DK, Goldstein SA, Brandt KD, O'Connor BL, Goulet RW, Albrecht M. A longitudinal study of subchondral plate and trabecular bone in cruciate-deficient dogs with osteoarthritis followed up for 54 months. Arthritis Rheum 1993;36:1460−7.
10. Hayami T, Pickarski M, Wesolowski GA, McClane J, Bone A, Destefano J, *et al*. Reduction of cartilage degeneration and prevention of osteophyte formation by alendronate in the rat anterior cruciate ligament transection model. Arthritis Rheum 2004;50:1193−206.
11. Brandt KD, Myers SL, Burr D, Albrecht M. Osteoarthritic changes in canine articular cartilage, subchondral bone, and synovium fifty-four months after transection of the anterior cruciate ligament. Arthritis Rheum 1991; 34:1560−70.
12. Pastoureau P, Leduc S, Chomel A, De Ceuninck F. Quantitative assessment of articular cartilage and subchondral bone histology in the meniscectomized guinea pig model of osteoarthritis. Osteoarthritis Cartilage 2003;11:412−23.
13. Fazzalari NL, Parkinson IH. Fractal properties of subchondral cancellous bone in severe osteoarthritis of the hip. J Bone Miner Res 1997;12:632−40.
14. Matsui H, Shimizu M, Tsuji H. Cartilage and subchondral bone interaction in osteoarthrosis of human knee joint: a histological and histomorphometric study. Microsc Res Tech 1997 May 15;37:333−42.
15. Kamibayashi L, Wyss UP, Cooke TD, Zee B. Trabecular microstructure in the medial condyle of the proximal tibia of patients with knee osteoarthritis. Bone 1995; 17:27−35.
16. Bobinac D, Spanjol J, Zoricic S, Maric I. Changes in articular cartilage and subchondral bone histomorphometry in osteoarthritic knee joints in humans. Bone 2003;32:284−90.
17. Burr DB, Radin EL. Microfractures and microcracks in subchondral bone: are they relevant to osteoarthrosis? Rheum Dis Clin North Am 2003 Nov;29:675−85.
18. Odgaard A, Gundersen HJ. Quantification of connectivity in cancellous bone, with special emphasis on 3-D reconstructions. Bone 1993;14:173−82.
19. Boyd SK, Muller R, Zernicke RF. Mechanical and architectural bone adaptation in early stage experimental osteoarthritis. J Bone Miner Res April 2002;17: 687−94.
20. Ding M, Odgaard A, Hvid I. Changes in the three-dimensional microstructure of human tibial cancellous bone in early osteoarthritis. J Bone Joint Surg Br 2003 Aug;85:906−12.
21. Peyrin F, Salome M, Nuzzo S, Cloetens P, Laval-Jeantet AM, Baruchel J. Perspectives in three-dimensional analysis of bone samples using synchrotron radiation microtomography. Cell Mol Biol 2000 Sep; 46:1089−102.
22. Nuzzo S, Peyrin F, Cloetens P, Baruchel J, Boivin G. Quantification of the degree of mineralization of bone in three dimensions using synchrotron radiation microtomography. Med Phys 2002;29:2672−81.
23. Engelke K, Graeff W, Meiss L, Hahn M, Delling G. High spatial resolution imaging of bone mineral using computed microtomography. Comparison with microradiography and undecalcified histologic sections. Invest Radiol 1993;28:341−9.
24. Bonse U, Busch F, Gunnewig O, Beckmann F, Pahl R, Delling G, *et al*. 3D computed X-ray tomography of human cancellous bone at 8 microns spatial and 10(−4) energy resolution. Bone Miner 1994;25:25−38.
25. Lane NE, Haupt D, Kimmel DB, Modin G, Kinney JH. Early estrogen replacement therapy reverses the rapid loss of trabecular bone volume and prevents further deterioration of connectivity in the rat. J Bone Miner Res 1999;14:206−14.
26. Peyrin F, Muller C, Carillon Y, Nuzzo S, Bonnassie A, Briguet A. Synchrotron radiation microCT: a reference tool for the characterization of bone samples. Adv Exp Med Biol 2001;496:129−42.
27. Nuzzo S, Lafage-Proust MH, Martin-Badosa E, Boivin G, Thomas T, Alexandre C, *et al*. Synchrotron radiation microtomography allows the analysis of three-dimensional microarchitecture and degree of mineralization of human iliac crest biopsy specimens: effects of etidronate treatment. J Bone Miner Res 2002;17:1372−82.
28. Lespessailles E, Jullien A, Eynard E, Harba R, Jacquet G, Ildefonse JP, *et al*. Biomechanical properties of human os calcanei: relationships with bone density and fractal evaluation of bone microarchitecture. J Biomech 1998;31:817−24.
29. Salome M, Peyrin F, Cloetens P, Odet C, Laval-Jeantet AM, Baruchel J, *et al*. A synchrotron radiation microtomography system for the analysis of trabecular bone samples. Med Phys 1999;26:2194−204.
30. Kinney JH, Lane NE, Haupt DL. *In vivo*, three-dimensional microscopy of trabecular bone. J Bone Miner Res 1995;10:264−70.
31. Whitehouse WJ. The quantitative morphology of anisotropic trabecu lar bone. J Microsc 1974;101(2): 153−68.
32. Parfitt AM, Drezner MK, Glorieux FH, Kanis JA, Malluche H, Meunier PJ, *et al*. Bone histomorphometry: standardization of nomenclature, symbols, and units. report of the ASBMR histomorphometry nomenclature committee. J Bone Miner Res 1987;595−610.
33. Hildebrand T, Laib A, Muller R, Dequeker J, Ruegsegger P. Direct three-dimensional morphometric analysis of human cancellous bone: microstructural data from spine, femur, iliac crest, and calcaneus. J Bone Miner Res 1999;14:1167−74.
34. Martin-Badosa E, Elmoutaouakkil A, Nuzzo S, Amblard D, Vico L, Peyrin F. A method for the automatic characterization of bone architecture in 3D mice microtomographic images. Comput Med Imaging Graph 2003;27:447−58.
35. Odgaard A, Kabel J, van Rietbergen B, Dalstra M, Huiskes R. Fabric and elastic principal directions of cancellous bone are closely related. J Biomech 1997;30:487−95.
36. Chang KP, Center JR, Nguyen TV, Eisman JA. Incidence of hip and other osteoporotic fractures in elderly men and women: Dubbo Osteoporosis Epidemiology Study. J Bone Miner Res 2004;19:532−6.
37. Li B, Aspden RM. Composition and mechanical properties of cancellous bone from the femoral head of patients with osteoporosis or osteoarthritis. J Bone Miner Res 1997;12:641−51.
38. Boyd SK, Muller R, Matyas JR, Wohl GR, Zernicke RF. Early morphometric and anisotropic change in periarticular cancellous bone in a model of experimental knee osteoarthritis quantified using microcomputed tomography. Clin Biomech 2000;15:624−31.
39. Newitt DC, Majumdar S, Van Rietbergen B, Ingersleben GV, Harris ST, Genant HK, *et al*. *In vivo*

assessment of architecture and micro-finite element analysis derived indices of mechanical properties of trabecular bone in the radius. Osteoporos Int 2002; 13:6–17.
40. Mosekilde L. Sex differences in age related loss of vertebral trabecular bone mass and structure biomechanical consequences. Bone 1989;10:425–32.
41. Singh M, Nagrath AR, Maini PS. Changes in trabecular pattern of the upper end of the femur as an index of osteoporosis. J Bone Joint Surg 1970;52A:457–67.
42. Jhamaria NL, Lal KB, Udawat M, Banerji P, Kabra SG. The trabecular pattern of the calcaneus as an index of osteoporosis. J Bone Joint Surg 1983;65:195–8.
43. Radin EL, Rose RM. Role of subchondral bone in the initiation and progression of cartilage damage. Clin Orthop 1986;213:34–40.
44. Ruegsegger P, Koller B, Muller R. A microtomographic system for the nondestructive evaluation of bone architecture. Calcif Tissue Int 1996;58:24–9.
45. Hara T, Tanck E, Homminga J, Huiskes R. The influence of microcomputed tomography threshold variations on the assessment of structural and mechanical trabecular bone properties. Bone 2002; 31:107–9.
46. Elmoutaouakkil A, Peyrin F, Elkafi J, Laval-Jeantet AM. Segmentation of cancellous bone from high-resolution computed tomography images: influence on trabecular bone measurements. IEEE Trans Med Imaging 2002; 21:354–62.
47. Boivin G, Meunier PJ. Changes in bone remodeling rate influence the degree of mineralization of bone. Connect Tissue Res 2002;43:535–7.
48. Grynpas MD, Alpert B, Katz I, Lieberman I, Pritzker KP. Subchondral bone in osteoarthritis. Calcif Tissue Int 1991;49:20–6.
49. Mansell JP, Bailey AJ. Abnormal cancellous bone collagen metabolism in osteoarthritis. J Clin Invest April 1998;15(101):1596–603.
50. Ferguson VL, Bushby AJ, Boyde A. Nanomechanical properties and mineral concentration in articular calcified cartilage and subchondral bone. J Anat 2003 Aug; 203:191–202.